

**Supersolid-like square- and honeycomb-lattice crystallization of droplets in a dipolar condensate**Luis E. Young-S. <sup>1,\*</sup> and S. K. Adhikari <sup>2,†</sup><sup>1</sup>*Grupo de Modelado Computacional, Facultad de Ciencias Exactas y Naturales, Universidad de Cartagena, 130014 Cartagena, Bolívar, Colombia*<sup>2</sup>*Instituto de Física Teórica, Universidade Estadual Paulista, 01.140-070 São Paulo, São Paulo, Brazil*

(Received 18 November 2021; accepted 1 March 2022; published 21 March 2022)

We demonstrate a supersolid-like spatially periodic square- and honeycomb-lattice crystallization of droplets in addition to the commonly studied triangular-lattice crystallization in a cylindrically symmetric quasi-two-dimensional trapped dipolar condensate, using a beyond-mean-field model including a quantum-fluctuation Lee-Huang-Yang-type interaction. These three types of crystallization of droplets may appear for the *same* atomic interaction and the *same* trap frequencies. The energies  $E$  of all three crystallizations as a function of the number  $N$  of atoms satisfy the universal scaling relation  $E \sim N^{0.4}$ , indicating that all three arrangements of the droplets should be energetically probable processes of phenomenological interest. The state of square-lattice crystallization may have the central site occupied or unoccupied, corresponding to a parity-symmetric or parity-antisymmetric state, respectively. The state of square-lattice crystallization with the occupied central site and the state of triangular-lattice crystallization, for a fixed  $N$ , constitute two quasidegenerate ground states, while the other states are low-lying excited states. This makes the square-lattice crystallization with the occupied central site an ideal candidate for future experimental observation.

DOI: [10.1103/PhysRevA.105.033311](https://doi.org/10.1103/PhysRevA.105.033311)**I. INTRODUCTION**

A supersolid [1–6] is a special form of quantum matter which exhibits a spatially ordered stable structure, as encountered in a solid crystal, breaking continuous translational invariance. A supersolid can also flow without friction as a superfluid, breaking continuous gauge invariance. Hence, contrary to the wisdom that frictionless flow is an exclusive property of a superfluid, a supersolid simultaneously possesses the properties of a superfluid and a solid. The search for supersolidity in  $^4\text{He}$  [7] was not conclusive [8]. However, there were theoretical suggestions for creating a supersolid in a dipolar Bose-Einstein condensate (BEC) [9–11], in a BEC with finite-range atomic interaction [12], and in a spin-orbit (SO)-coupled spinor BEC [13]. The study of supersolids has recently gained new impetus among researchers in low-temperature physics after the experimental observation of supersolids in a dipolar BEC [14,15] and in an SO-coupled pseudo-spin-1/2 spinor BEC [16].

Recently, a spatially periodic state displaying a stripe pattern in density, known as a superstripe state because of its supersolid-like properties, was experimentally observed in an SO-coupled pseudo-spin-1/2 BEC of  $^{23}\text{Na}$  atoms [16]. In quasi-two-dimensional (quasi-2D) uniform and trapped SO-coupled spin-2 [17], spin-1 [18,19], and pseudo-spin-1/2 [20] spinor BECs, the formation of *square- and triangular-lattice* patterns in density was demonstrated in theoretical studies in addition to the superstripe state [13,16]. In a strongly dipolar BEC, for an appropriate mixture of dipolar and contact

interactions and for a number of atoms  $N$  beyond a critical value, high-density droplet formation was observed experimentally in a dipolar BEC under a strong trap of  $^{164}\text{Dy}$  [15] and  $^{168}\text{Er}$  [21] atoms and was studied theoretically [22,23]. In the framework of a mean-field model employing the Gross-Pitaevskii (GP) equation, a dipolar BEC collapses for strong dipolar interaction beyond a critical value, and a Lee-Huang-Yang-type [24] (LHY-type) beyond-mean-field quantum-fluctuation interaction [25,26] is necessary in theoretical studies to stabilize a strongly dipolar droplet against collapse [11]. As the number of atoms  $N$  in a trapped dipolar BEC is increased so that the density of atoms reaches a critical value, due to the dipolar interaction, the condensate shrinks to a very small size. However, it cannot collapse due to the quantum-fluctuation LHY interaction, and a droplet is formed. The size of the droplet is much smaller than the harmonic oscillator trap lengths. Such droplets can accommodate a maximum number of atoms [22] for given harmonic trap frequencies to attain a critical density of atoms in the condensate. In spite of the name droplet, the present dipolar BEC droplets in a strong trap are different from recently observed [27,28] nondipolar binary BEC droplets in free space. Nevertheless, in both cases, the collapse is arrested by a beyond-mean-field quantum-fluctuation LHY interaction.

For a sufficiently large  $N$ , in a quasi-one-dimensional (quasi-1D) trapped dipolar BEC, spontaneous periodic crystallization of droplets along a straight line was observed in different experiments on  $^{164}\text{Dy}$  [29–31],  $^{162}\text{Dy}$  [32–34], and  $^{166}\text{Er}$  [30,31] atoms and was confirmed in related theoretical studies [35,36], whereas in a quasi-2D trapped dipolar BEC of  $^{164}\text{Dy}$  atoms, crystallization of droplets on a periodic triangular lattice was observed experimentally [14,37] and was established in theoretical studies [38–42]. In addition to this

\*lyoung@unicartagena.edu.co

†sk.adhikari@unesp.br; professores.ift.unesp.br/sk.adhikari/

periodic triangular-lattice state, in a trapped quasi-2D dipolar BEC, the formation of honeycomb, stripe, and other periodic structures in density and not crystallization of droplets has also been predicted [40–43] in theoretical studies. Nevertheless, in many of these investigations, especially in the numerical studies on a truncated finite system, the supersolidity of the system has never been rigorously established [44]. One needs to show the spontaneous breaking of gauge symmetry (which gives the superfluid order parameter) and the spontaneous breaking of translational symmetry in the same system. Lacking a rigorous demonstration of supersolidity, we prefer to call these periodic states supersolid-like states in this paper as in similar studies on quasi-2D SO-coupled spinor BECs [17,19].

Following the 1D crystallization of dipolar droplets along a straight line in a quasi-1D trap [29–36], the natural crystallization in two dimensions is the square-lattice arrangement of droplets, which has not yet been observed in experiments or predicted theoretically. In this paper, using a beyond-mean-field model including the quantum-fluctuation LHY interaction [25,26] for a three-dimensional (3D) trapped dipolar BEC, we explicitly demonstrate supersolid-like spatially periodic square- and honeycomb-lattice crystallization of droplets in the  $x$ - $y$  plane perpendicular to the polarization  $z$  direction for an appropriate mixture of dipolar and contact interactions in a quasi-2D trap in addition to the triangular-lattice crystallization of droplets found in different theoretical [38,40] and experimental [14,37] investigations. We found that the symmetry of the final state is sensitive to the initial state employed in numerical simulation. A final state with a specific symmetry—a square, triangular, or a honeycomb lattice—can easily be obtained with the use of an initial state with the same symmetry. No such supersolid-like state can be obtained in a trapped BEC with isotropic contact interaction. In the case of dipolar interaction, a single droplet can be stable for a maximum number of atoms. As the number of atoms is increased further, multiple droplets are generated, and due to the interplay between the dipolar repulsion in the  $x$ - $y$  plane and the external trapping potential, a supersolid-like arrangement of droplets is formed.

In this study we find two distinct types of square-lattice arrangements of dipolar droplets in a circularly symmetric quasi-2D trapped dipolar BEC, e.g., with the central site at  $x = y = 0$  occupied or vacant. In the case when the central site is occupied (unoccupied) by a droplet, the wave function is parity symmetric (parity antisymmetric). In the first type we find 9, 25, 49, . . . droplets arranged on  $3 \times 3$ ,  $5 \times 5$ ,  $7 \times 7$ , . . . arrays, whereas in the second type we find 4, 16, 36, . . . droplets arranged on  $2 \times 2$ ,  $4 \times 4$ ,  $6 \times 6$ , . . . arrays (see Fig. 2 below). Like usual parity-antisymmetric states, the square-lattice crystallization with a vacant central site is an excited state. We also numerically investigate the triangular-lattice arrangement of droplets studied previously. In addition to the triangular and square-lattice arrangements, we also demonstrate a clean honeycomb-lattice arrangement of droplets. A honeycomb lattice is a special case of a triangular lattice with missing droplets at the centers of adjacent hexagons. Of these different possibilities, the triangular-lattice arrangement of droplets and the square-lattice arrangement with an occupied central site constitute two quasidegenerate

stable ground states. The honeycomb-lattice and square-lattice arrangements with a vacant central site have slightly larger energies and are excited states.

We also calculated the energies of the different states and established a universal scaling relation between the energy per atom  $E$  of the supersolid-like crystallization of droplets on square, honeycomb, and triangular lattices and the number of atoms  $N$  independent of the type of lattice, which implies that these three periodic crystallizations of droplets are all equally probable energetically. Moreover, the three different crystallizations of droplets appear for the same atomic contact and dipolar interactions and for the same trap frequencies. Hence, all these periodic crystallizations of droplets should be of experimental interest. With this in mind, in this paper, we have employed the same confining trap frequencies and a similar number of  $^{164}\text{Dy}$  atoms as in previous experimental [37] and theoretical [38] studies on the triangular-lattice formation of dipolar droplets. The number of droplets  $n_d$  is found to increase approximately linearly with  $N$ .

In Sec. II we present the beyond-mean-field model including the quantum-fluctuation LHY interaction in the GP equation. The time-independent version of this equation is also obtained from a variational rule using a time-independent energy functional. In Sec. III we present the numerical results for stationary states with three types of periodic arrays of droplets, e.g., a square lattice, triangular lattice, and honeycomb lattice, in a trapped dipolar BEC. Finally, in Sec. IV we present a summary of our findings.

## II. BEYOND-MEAN-FIELD MODEL

In this paper we base our study on a 3D beyond-mean-field model including the quantum-fluctuation LHY interaction. We consider a BEC of  $N$  dipolar atoms polarized along the  $z$  axis, of mass  $m$  each, interacting through the following atomic dipolar and contact interactions [45–47]:

$$V(\mathbf{R}) = \frac{\mu_0 \mu^2}{4\pi} \frac{1 - 3 \cos^2 \theta}{|\mathbf{R}|^3} + \frac{4\pi \hbar^2 a}{m} \delta(\mathbf{R}), \quad (1)$$

where  $a$  is the scattering length,  $\mu_0$  is the permeability of vacuum,  $\mu$  is the magnetic dipole moment of each atom,  $\mathbf{R} = \mathbf{r} - \mathbf{r}'$  is the vector joining two dipoles placed at  $\mathbf{r} \equiv \{x, y, z\}$  and  $\mathbf{r}' \equiv \{x', y', z'\}$ , and  $\theta$  is the angle made by  $\mathbf{R}$  with the  $z$  axis. The strength of dipolar interaction is given by the dipolar length

$$a_{\text{dd}} = \frac{\mu_0 \mu^2 m}{12\pi \hbar^2}. \quad (2)$$

The dimensionless ratio

$$\varepsilon_{\text{dd}} \equiv \frac{a_{\text{dd}}}{a} \quad (3)$$

determines the strength of the dipolar interaction relative to the contact interaction and controls many properties of a dipolar BEC.

A dipolar BEC is described by the following 3D beyond-mean-field GP equation including the quantum-fluctuation

LHY interaction [23,38,45–47]:

$$\begin{aligned}
 i\hbar \frac{\partial \psi(\mathbf{r}, t)}{\partial t} = & \left[ -\frac{\hbar^2}{2m} \nabla^2 + U(\mathbf{r}) + \frac{4\pi \hbar^2}{m} aN |\psi(\mathbf{r}, t)|^2 \right. \\
 & + \frac{3\hbar^2}{m} a_{\text{dd}} N \int \frac{1 - 3 \cos^2 \theta}{|\mathbf{R}|^3} |\psi(\mathbf{r}', t)|^2 d\mathbf{r}' \\
 & \left. + \frac{\gamma_{\text{QF}} \hbar^2}{m} |\psi(\mathbf{r}, t)|^3 \right] \psi(\mathbf{r}, t), \quad (4)
 \end{aligned}$$

where  $U(\mathbf{r}) = \frac{1}{2}m(\omega_x^2 x^2 + \omega_y^2 y^2 + \omega_z^2 z^2)$  is the trap with angular frequencies  $\omega_x \equiv 2\pi f_x$ ,  $\omega_y \equiv 2\pi f_y$ , and  $\omega_z \equiv 2\pi f_z$  along the  $x$ ,  $y$ , and  $z$  directions, respectively, and the wave function is normalized as  $\int |\psi(\mathbf{r}, t)|^2 d\mathbf{r} = 1$ . The coefficient of the beyond-mean-field quantum-fluctuation LHY term  $\gamma_{\text{QF}}$  is given by [23,25,26]

$$\gamma_{\text{QF}} = \frac{128}{3} \sqrt{\pi a^5} Q_5(\varepsilon_{\text{dd}}), \quad (5)$$

where the auxiliary function

$$Q_5(\varepsilon_{\text{dd}}) = \int_0^1 dx (1 - x + 3x\varepsilon_{\text{dd}})^{5/2} \quad (6)$$

can be evaluated as [23]

$$\begin{aligned}
 Q_5(\varepsilon_{\text{dd}}) = & \frac{(3\varepsilon_{\text{dd}})^{5/2}}{48} \text{Re} \left[ (8 + 26\varepsilon + 33\varepsilon^2) \sqrt{1 + \varepsilon} \right. \\
 & \left. + 15\varepsilon^3 \ln \left( \frac{1 + \sqrt{1 + \varepsilon}}{\sqrt{\varepsilon}} \right) \right], \quad \varepsilon = \frac{1 - \varepsilon_{\text{dd}}}{3\varepsilon_{\text{dd}}} \quad (7) \\
 \approx & 1 + \frac{3}{2} \varepsilon_{\text{dd}}^2, \quad (8)
 \end{aligned}$$

where  $\text{Re}$  denotes the real part. In the present study we use the exact expression (7). Actually, for  $\varepsilon_{\text{dd}} > 1$ ,  $Q_5$  is complex, and its small imaginary part will be neglected, as in other studies [37,38], in the present study of stationary droplet states. The use of the approximate expression (8), such as in Refs. [39,42], leads to qualitatively acceptable results for droplet and droplet-lattice formation but may lead to sizable error in the quantitative estimate of energy, size, etc., of the final state.

Equation (4) can be reduced to the following dimensionless form by scaling lengths in units of  $l = \sqrt{\hbar/m\omega_z}$ , time in units of  $\omega_z^{-1}$ , energy in units of  $\hbar\omega_z$ , and density  $|\psi|^2$  in units of  $l^{-3}$ :

$$\begin{aligned}
 i \frac{\partial \psi(\mathbf{r}, t)}{\partial t} = & \left[ -\frac{1}{2} \nabla^2 + \frac{1}{2} \left( \frac{f_x^2}{f_z^2} x^2 + \frac{f_y^2}{f_z^2} y^2 + z^2 \right) \right. \\
 & + 3a_{\text{dd}} N \int \frac{1 - 3 \cos^2 \theta}{|\mathbf{R}|^3} |\psi(\mathbf{r}', t)|^2 d\mathbf{r}' \\
 & \left. + 4\pi a N |\psi(\mathbf{r}, t)|^2 + \gamma_{\text{QF}} N^{3/2} |\psi(\mathbf{r}, t)|^3 \right] \psi(\mathbf{r}, t). \quad (9)
 \end{aligned}$$

Equation (9) can also be obtained from the variational rule

$$i \frac{\partial \psi}{\partial t} = \frac{\delta E}{\delta \psi^*} \quad (10)$$

with the following energy functional (energy per atom):

$$\begin{aligned}
 E = \int d\mathbf{r} & \left[ \frac{|\nabla \psi(\mathbf{r})|^2}{2} + \frac{1}{2} \left( \frac{f_x^2}{f_z^2} x^2 + \frac{f_y^2}{f_z^2} y^2 + z^2 \right) |\psi(\mathbf{r})|^2 \right. \\
 & + \frac{3}{2} a_{\text{dd}} N |\psi(\mathbf{r})|^2 \int \frac{1 - 3 \cos^2 \theta}{R^3} |\psi(\mathbf{r}')|^2 d\mathbf{r}' \\
 & \left. + 2\pi N a |\psi(\mathbf{r})|^4 + \frac{2\gamma_{\text{QF}}}{5} N^{3/2} |\psi(\mathbf{r})|^5 \right] \quad (11)
 \end{aligned}$$

for a stationary state.

### III. NUMERICAL RESULTS

We solve partial differential equation (9) for a dipolar BEC numerically using the FORTRAN and C programs [46] or their open-multiprocessing versions [48] using the split-time-step Crank-Nicolson method [49] employing the imaginary-time propagation rule. Often, the intensity of the system has a large extension in the  $x$ - $y$  plane, and it is appropriate to take a larger number of discretization steps along the  $x$  and  $y$  directions compared to the steps along the  $z$  direction. It is problematic to treat numerically the nonlocal dipolar interaction integral in the beyond-mean-free model (9) in configuration space due to the  $1/|\mathbf{R}|^3$  term. To circumvent this problem, this term is evaluated in momentum space by a Fourier transformation using a convolution identity [46], which is advantageous numerically due to the smooth behavior of this term in momentum space. The Fourier transformation of the dipolar potential in three dimensions can be found analytically, enhancing the accuracy of the numerical procedure.

Instead of presenting results in dimensionless units, we prefer to relate our results to the recent experimental [37] and related theoretical [38] studies on dipolar droplets using  $^{164}\text{Dy}$  atoms. For the appearance of droplets we need a strongly dipolar atom with  $\varepsilon_{\text{dd}} > 1$  [14]. In this study we take  $a = 85a_0$ , close to its experimental estimate  $a = (92 \pm 8)a_0$  [50], and  $a_{\text{dd}} = 130.8a_0$ , where  $a_0$  is the Bohr radius; consequently,  $\varepsilon_{\text{dd}} = 1.5388 \dots > 1$ . This value of scattering length is close to the scattering lengths  $a = 88a_0$  [37,38] and  $a = 70a_0$  [39] used in some other studies of quantum droplets in a quasi-2D dipolar BEC. The trap frequencies along the  $x$ ,  $z$ , and  $y$  directions are taken to be  $f_x = 33$  Hz,  $f_z = 167$  Hz, and  $f_y = 110$  Hz (trap  $U_A$ ), 60 Hz (trap  $U_B$ ), and 33 Hz (trap  $U_C$ ) as in recent experimental [37] and theoretical [38] investigations of triangular-lattice crystallization of droplets. Trap  $U_A$  is of the quasi-1D type along the  $x$  direction ( $f_y, f_z \gg f_x$ ), and trap  $U_C$  is of the cylindrically symmetric quasi-2D type in the  $x$ - $y$  plane ( $f_x = f_y \ll f_z$ ). Trap  $U_B$  is an asymmetric trap ( $f_x \neq f_y \neq f_z$ ) in the transition domain from the quasi-1D to the quasi-2D type. With these parameters—frequencies for trap  $U_C$  and scattering length  $a$ —we found simultaneously square-, triangular-, and honeycomb-lattice crystallizations of droplets in a trapped quasi-2D dipolar BEC of  $^{164}\text{Dy}$  atoms, and these three different arrangements of droplets were found to have similar energies for a fixed  $N$ . In this study we have  $m(^{164}\text{Dy}) = 164 \times 1.66054 \times 10^{-27}$  kg,  $\hbar = 1.0545718 \times 10^{-34}$  m<sup>2</sup> kg/s, and  $\omega_z = 2\pi \times 167$  Hz, and consequently, the unit of length  $l = \sqrt{\hbar/m\omega_z} = 0.607$   $\mu\text{m}$ .

For efficient and quick convergence of a single-droplet state or of a lattice-droplet arrangement in an imaginary-time calculation, an appropriate choice of the initial state is essential. The numerical simulation of a single-droplet state was started with a Gaussian wave function of small width:  $\phi(\mathbf{r}) \sim e^{-x^2-y^2} e^{-z^2/\alpha^2}$ , with the width parameter  $\alpha \approx 4$ . The numerical simulation for a lattice-droplet state was started by many Gaussian droplets arranged on a desired lattice. For example, a 49-droplet square-lattice state [see Fig. 3(f) below] was started with the following analytic function:

$$\phi(\mathbf{r}) \sim \sum_{i,j=0}^{\pm 1, \pm 2, \pm 3} e^{-(x+\beta i)^2 - (y+\beta j)^2} e^{-z^2/\alpha^2}, \quad (12)$$

with the lattice length  $\beta \approx 5$ . The calculations with honeycomb- and triangular-lattice states were initiated similarly using analytic initial functions with the droplets arranged appropriately.

To find a 1D crystallization of droplets, we consider 25 000  $^{164}\text{Dy}$  atoms in the quasi-1D trap  $U_A$ . With this trap  $f_x \ll f_y, f_z$ , the dipolar BEC crystallizes in droplets along the  $x$  axis. The converged final state in this case can be obtained by imaginary-time simulation using an initial Gaussian wave function. However, the convergence is quicker if we use an analytic wave function for a few droplets (three or five) periodically arranged along the  $x$  direction with a mutual separation  $\beta$  and symmetrically placed around the occupied  $x = 0$  site. A contour plot of the  $z = 0$  section of the 3D density  $|\psi(x, y, 0)|^2$  is shown in Fig. 1(a) with three droplets placed symmetrically around  $x = 0$  (a parity-symmetric state). For the same set of parameters, there is a parity-antisymmetric excited state of higher energy with four droplets placed symmetrically around  $x = 0$ , but with the central site at  $x = 0$  unoccupied (not shown here; see Fig. 1(a) of Ref. [38]). In trap  $U_B$ , as trap frequency  $f_y$  is reduced to 60 Hz, the number of droplets for  $N = 25\,000$  reduces from three to one, as shown in Fig. 1(b), where we use the final converged wave function of Fig. 1(a) as the initial state in the imaginary-time simulation. A droplet will be formed when the density is larger than a critical density. Inside a droplet the dipolar interaction is so strong that the dipolar BEC becomes quasi-1D along the  $z$  direction with a small transverse section. A weaker trap in Fig. 1(b), compared to that in Fig. 1(a), requires a larger number of atoms to attain the critical density required for droplet formation [40]. Consequently, a droplet in the weaker trap  $U_B$  can accommodate a larger number of atoms, and the number of droplets is reduced from three in trap  $U_A$  to one in trap  $U_B$ . In the cylindrically symmetric quasi-2D weak trap  $U_C$ , the central density for 25 000 atoms is smaller than the threshold for droplet formation; consequently, no droplets can be formed, and the density is of normal Gaussian type [see Fig. 1(c)], with a large increase in the size of the condensate. However, for  $N > N_{\text{cr}} = 33\,000$  the critical density for the formation of a droplet is attained in trap  $U_C$ , and a droplet can be formed as shown in Fig. 1(d) for  $N = 40\,000$ .

We illustrate the quasi-1D to quasi-2D transition of a square-lattice arrangement of droplets for a fixed number of atoms  $N = 70\,000$  in Figs. 1(e)–1(g) for traps  $U_A$ ,  $U_B$  and  $U_C$ , respectively, through a contour plot of 2D density  $|\psi(x, y, 0)|^2$  in the  $x$ - $y$  plane. In the quasi-1D trap  $U_A$ , we have a linear

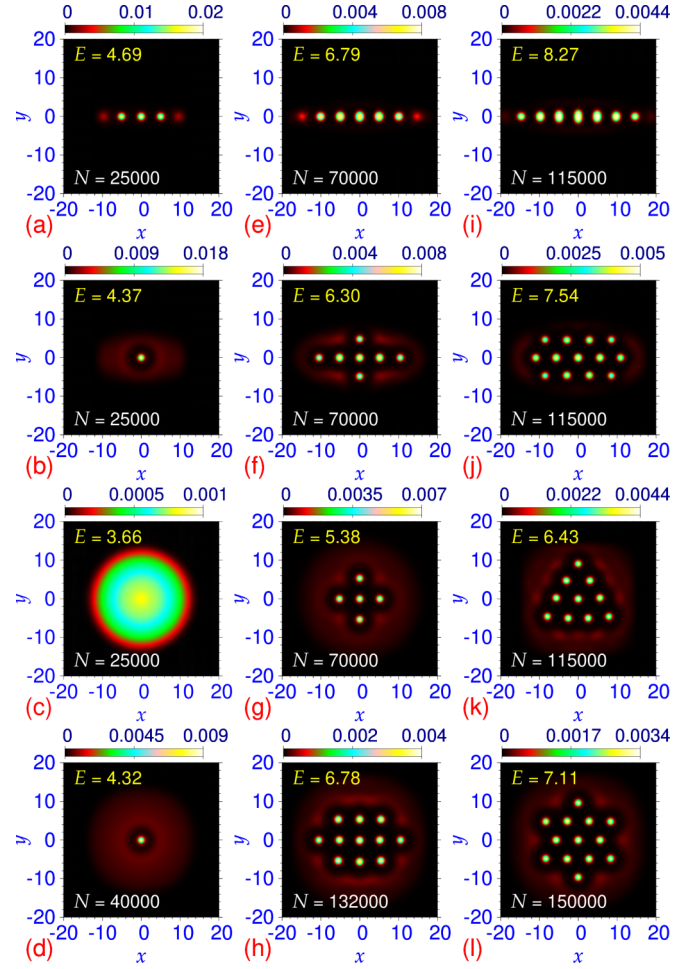


FIG. 1. Contour plot of the density  $|\psi(x, y, 0)|^2$  of a dipolar BEC of  $N = 25\,000$   $^{164}\text{Dy}$  atoms in traps (a)  $U_A$  ( $f_y = 110$  Hz), (b)  $U_B$  ( $f_y = 60$  Hz), and (c)  $U_C$  ( $f_y = 33$  Hz). (d) The same for  $N = 40\,000$  atoms in trap  $U_C$ . The same for  $N = 70\,000$  atoms in traps (e)  $U_A$ , (f)  $U_B$ , and (g)  $U_C$ . (h) The same for  $N = 132\,000$  atoms in trap  $U_C$ . The same for  $N = 115\,000$  atoms in traps (i)  $U_A$ , (j)  $U_B$ , and (k)  $U_C$ . (l) The same for  $N = 150\,000$  atoms in trap  $U_C$ . All plots are labeled by the respective  $E$  and  $N$  values. In the first column we illustrate the formation of a single droplet; in the second column we illustrate the formation of a square-lattice arrangement of droplets, and in the third column we illustrate that of a triangular-lattice arrangement of droplets. Other parameters in all calculations are  $f_x = 33$  Hz,  $f_z = 167$  Hz,  $a = 85a_0$ ,  $a_{\text{dd}} = 130.8a_0$ . The plotted quantities in all panels are dimensionless; the length scale  $l \equiv \sqrt{\hbar/m\omega_z} = 0.607 \mu\text{m}$ .

chain of droplets in Fig. 1(e), and in the quasi-2D trap  $U_C$ , an  $x$ - $y$ -symmetric arrangement of droplets is obtained, as shown in Fig. 1(g). An arrangement of droplets in the quasi-1D to quasi-2D transition domain in trap  $U_B$  is illustrated in Fig. 1(f). The number of droplets in a specific trap increases with  $N$ , as shown in Fig. 1(h) for  $N = 132\,000$  in trap  $U_C$  with 11 droplets compared to 5 droplets in Fig. 1(g) for  $N = 70\,000$ . The quasi-1D to quasi-2D transition of the triangular-lattice arrangement of droplets for  $N = 115\,000$  in Figs. 1(i)–1(k) for traps  $U_A$ ,  $U_B$ , and  $U_C$ , respectively, is considered next through a contour plot of 2D density  $|\psi(x, y, 0)|^2$  in the  $x$ - $y$

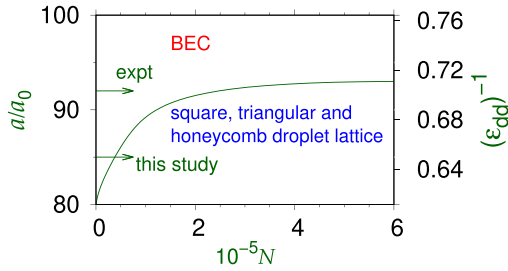


FIG. 2. The  $a/a_0$  versus  $N$  phase plot of droplet formation in trap  $U_C$  illustrating the square-, triangular- and honeycomb-lattice states. The region marked “BEC” represents a normal BEC of the type displayed in Fig. 1(c), where no droplet can be formed.

plane. In the quasi-1D trap  $U_A$ , again, we have a linear array of droplets in Fig. 1(i), and a triangular lattice of droplets in the quasi-2D trap  $U_C$  is displayed in Fig. 1(k). An intermediate triangular-lattice arrangement of droplets in trap  $U_B$  in the transition from quasi-1D to quasi-2D is presented in Fig. 1(j). In the quasi-1D trap  $U_A$ , the number of droplets  $n_d$  increases with  $N$ , as can be found from Figs. 1(a), 1(e) and 1(i). In the quasi-2D trap  $U_C$ , in general,  $n_d$  also increases with  $N$  [compare Figs. 1(g), 1(k) 1(h), and 1(l) with 5, 10, 11, and 13 droplets for  $N = 70\,000$ , 115 000, 132 000, 150 000, respectively]. The number of droplets is roughly proportional to the number of atoms. In Figs. 1(k) and 1(l) we find that a triangle-shaped triangular lattice has changed to a star-shaped triangular lattice with the increase of  $N$  in the same trap  $U_C$ .

In all cases, a cloud of atoms is found surrounding the lattice arrangement of droplets. It was not possible to avoid this cloud; if the calculation is repeated with a smaller  $N$ , the droplets at the four corners start to disappear, leaving the cloud intact. A similar cloud was also found in other theoretical [38–40] and experimental [37] investigations. After having established the formation of dipolar droplets of different symmetries, we now present an  $a/a_0$  versus  $N$  phase plot for droplet formation in trap  $U_C$  (our study will be confined to this quasi-2D trap) in Fig. 2, where the experimental scattering length  $a = 92a_0$  [50] and the present scattering length  $a = 85a_0$  are marked by arrows. This phase plot bears some similarity to the phase plot presented in Fig. 3 of Ref. [40] for  $a_{dd} = 130a_0$  in spite of the different trap frequencies in that reference. Although the region of droplet formation of Ref. [40] is quite similar to that in Fig. 2, only triangular-lattice formation is reported in Ref. [40]. Here we show that it is possible to have periodic square-, honeycomb-, and triangular-lattice arrangements of droplets in the same region. The stripe and honeycomb structures (and not the honeycomb-lattice droplet as reported in this paper) of Fig. 3 of Ref. [40] are possible beyond  $N = 6 \times 10^5$ , which is not considered in Fig. 2. In this study, we employ  $a = 85a_0$  and a large  $N$  deep inside the region of droplet formation in Fig. 2, where a large number of droplets can be formed.

To study the square-lattice crystallization of droplets in the cylindrically symmetric quasi-2D trap  $U_C$  we note that there are two types of square-lattice crystallization: an even number of droplets on each side of the square (with  $2 \times 2 =$

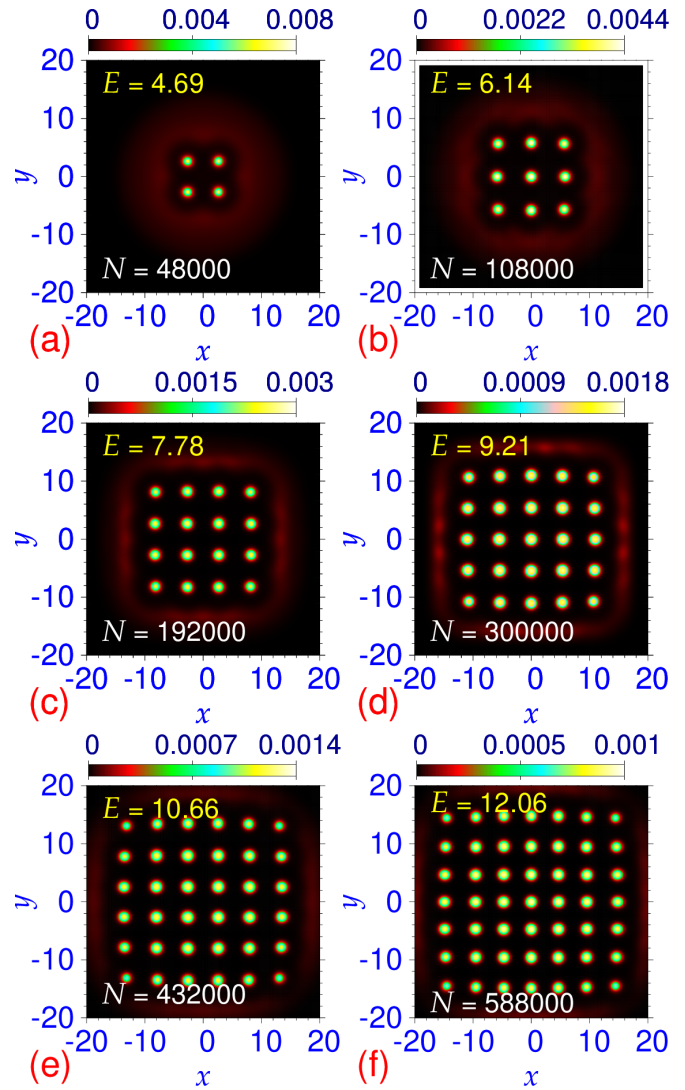


FIG. 3. Contour plot of the density  $|\psi(x, y, 0)|^2$  of square-lattice crystallization of 4, 9, 16, 25, 36, and 49 droplets, respectively, for (a)  $N = 48\,000$ , (b)  $N = 108\,000$ , (c)  $N = 192\,000$ , (d)  $N = 300\,000$ , (e)  $N = 432\,000$ , and (f)  $N = 588\,000$  in trap  $U_C$ .

4,  $4 \times 4 = 16$ ,  $6 \times 6 = 36$ , etc., droplets) and an odd number of droplets on each side of the square (with  $3 \times 3 = 9$ ,  $5 \times 5 = 25$ ,  $7 \times 7 = 49$ , etc., droplets); the corresponding density  $|\psi(x, y, 0)|^2$  in trap  $U_C$  is plotted in Figs. 3(a)–3(f) for  $N = 48\,000$ , 108 000, 192 000, 300 000, 432 000, and 588 000, respectively. For a symmetric distribution of the droplets, for the first (second) type, the central site at  $x = y = 0$  has to be vacant (occupied), corresponding to a parity-antisymmetric (parity-symmetric) state. All states are obtained by imaginary-time simulation using an analytic initial wave function on a square lattice with lattice spacing  $\beta$  [see Eq. (12)]. The appropriate  $N$  per droplet in a calculation for an efficient square-lattice formation was found to be of the order of 12 000. For a smaller  $N$ , the droplets at the corners may disappear, and for a larger  $N$ , an intense cloud forms around the droplets. With a further increase in the number of atoms, multiple (about two to four) droplets will form, thus reducing

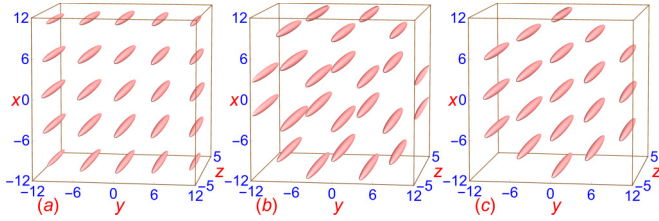


FIG. 4. Isodensity contour of the 3D density  $|\psi(x, y, z)|^2$  for (a) the square-lattice crystallization in Fig. 3(d) for  $N = 300\,000$ , (b) the honeycomb-lattice crystallization in Fig. 5(b) for  $N = 264\,000$ , and (c) the triangular-lattice crystallization in Fig. 6(b) for  $N = 228\,000$  in trap  $U_C$ .

the cloud. In Fig. 4(a) we display the isodensity contour of density  $|\psi(x, y, z)|^2$  for the square-lattice crystallization in Fig. 3(d).

A numerical simulation of the honeycomb-lattice crystallization of droplets needed much more care than the square- and triangular-lattice arrangements of droplets. This is because this arrangement is basically a triangular-lattice arrangement of droplets with a missing droplet at the center of all closed adjacent hexagons, and if the initial state is not properly chosen, the imaginary-time numerical simulation may converge to the triangular-lattice arrangement of droplets, filling in the vacant positions at the center of the closed hexagons with droplets. The densities of the honeycomb-lattice crystallization for 6 and 24 droplets in trap  $U_C$  are displayed in Figs. 5(a) and 5(b), respectively, for  $N = 72\,000$  and  $264\,000$ . In Fig. 4(b) we present the isodensity contour of the 3D density  $|\psi(x, y, z)|^2$  for the honeycomb-lattice crystallization in Fig. 5(b).

Finally, we investigate the triangular-lattice crystallization of droplets in trap  $U_C$ . In Figs. 6(a), 6(b) and 6(c) we display the contour plot of the density  $|\psi(x, y, 0)|^2$  of the triangular-lattice crystallization for 7, 19, and 37 droplets in trap  $U_C$  for  $N = 84\,000$ ,  $228\,000$ , and  $444\,000$ , respectively, calculated using an initial state with similar symmetry properties. In Fig. 4(c) we display the isodensity contour of the density  $|\psi(x, y, z)|^2$  for the triangular-lattice crystallization in Fig. 6(b). It is pertinent to ask the following: of the states of different arrangements of dipolar droplets, which is the

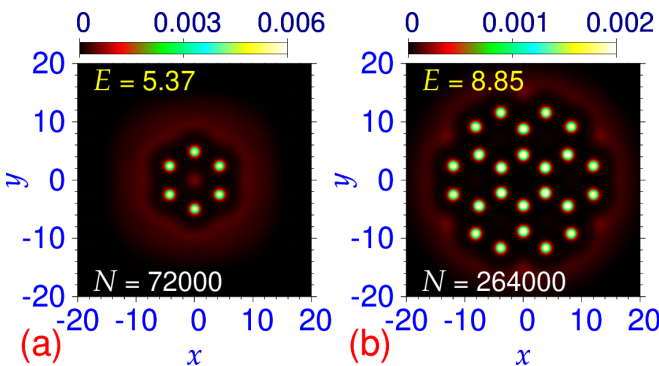


FIG. 5. Contour plot of the density  $|\psi(x, y, 0)|^2$  of the honeycomb-lattice crystallization of droplets for (a)  $N = 72\,000$  and (b)  $N = 264\,000$  in trap  $U_C$ .

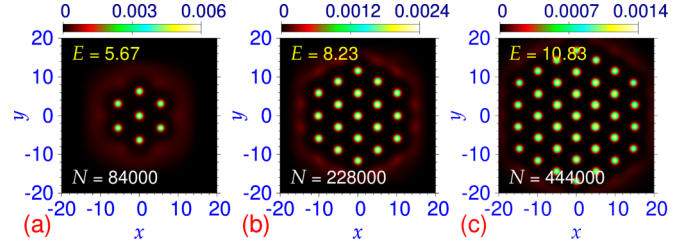


FIG. 6. Contour plot of the density  $|\psi(x, y, 0)|^2$  of the triangular-lattice crystallization of droplets for (a)  $N = 84\,000$ , (b)  $N = 228\,000$ , and (c)  $N = 444\,000$  in trap  $U_C$ .

ground state(s) and which are the excited states? There are two types of arrangement of droplets: one with the central site at  $x = y = 0$  occupied (the square lattice with an odd number of droplets and the triangular lattice) and one with the central site vacant (the square lattice with an even number of droplets and the honeycomb lattice). We find that the first of these types forms quasidegenerate ground states and the second type forms low-lying excited states. To demonstrate this claim we display in Figs. 7(a)–7(c) contour plots of the density  $|\psi(x, y, 0)|^2$  for  $N = 264\,000$  for triangular-lattice symmetry and two types of square-lattice symmetries. We find from Figs. 6(b) and 7(a) that we can have a 19-droplet triangular-lattice state for  $N = 228\,000$  and  $N = 264\,000$ , respectively; with the increased  $N$  in Fig. 7(a) we have an increased density of the atom cloud. Similarly, in Figs. 3(d) and 7(c) we find a 25-droplet square-lattice state for  $N = 300\,000$  and  $N = 264\,000$ , respectively. In this case with larger  $N$  in Fig. 3(d), we have an increased density of the atom cloud. From Figs. 7 and 5(b), for a fixed  $N = 264\,000$ , we find that the parity-symmetric square-lattice state with an occupied central site [Fig. 7(c)] and the triangular-lattice state [Fig. 7(a)] constitute the quasidegenerate ground states of energy  $E = 8.77$  and  $E = 8.78$ , respectively. The parity-antisymmetric square-lattice state with vacant central site [ $E = 8.80$ ; Fig. 7(b)] and the honeycomb-lattice state [ $E = 8.85$ ; Fig. 5(b)] are low-lying excited states. A similar result was found to be true for a few other  $N$  values (the details are not reported in this paper). In addition to the states of droplet arrangements on periodic lattices, which are highlighted in this paper, there could also be states of droplet arrangements with no specific symmetry. For a specific trap and for a fixed  $N$  all these states have nearby energies (not illustrated in this paper). In addition to

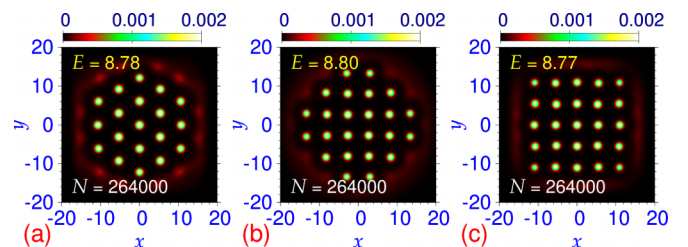


FIG. 7. Contour plot of the density  $|\psi(x, y, 0)|^2$  of (a) the triangular-lattice crystallization, (b) the square-lattice crystallization with a vacant central site, and (c) the square-lattice crystallization with an occupied central site for  $N = 264\,000$  in trap  $U_C$ .

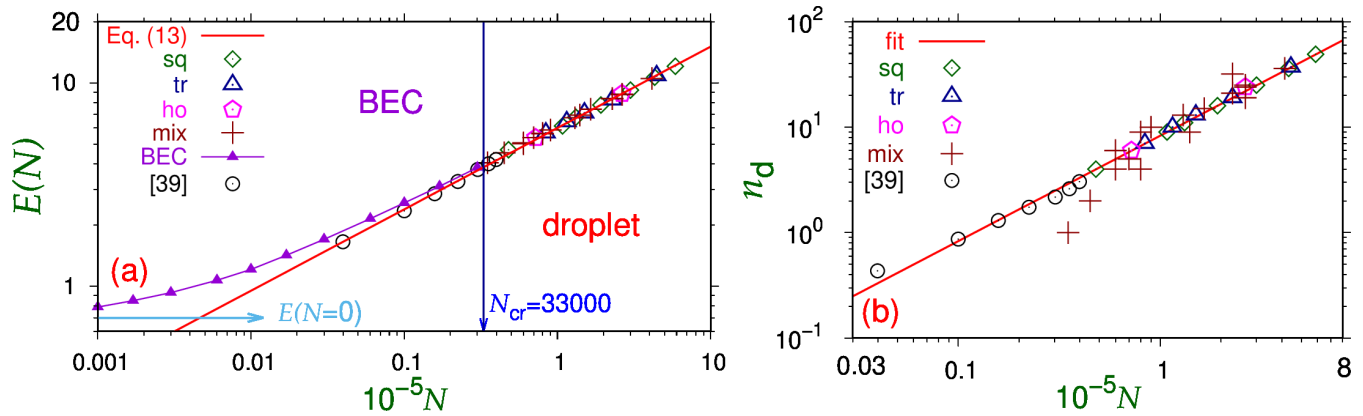


FIG. 8. (a) Energy per atom  $E$  and (b) number of droplets  $n_d$  versus  $N$  for all lattice states in trap  $U_C$  on log-log scale; sq: square-lattice states in Figs. 1(g), 1(h) and 3; tr: triangular-lattice states in Figs. 1(k), 1(l) and 6; ho: honeycomb-lattice states in Fig. 5; mix: the states presented in Fig. 7 and a few more not shown in this paper; BEC: normal BEC superfluid for smaller  $N$  [states of the type presented in Fig. 1(c)]; [39]: one- to seven-droplet states from Fig. 2(a) of [39] employing  $f_x = f_y = 60$  Hz,  $f_z = 300$  Hz,  $a = 70a_0$ , and approximation (8) in arbitrary units. The points are numerical results, and the straight lines labeled (a) “Eq. (13)” and (b) “fit” are the scaling relations  $E \approx 0.06 \times N^{0.4}$  and  $n_d \approx N/12000$ , respectively. The regions of normal BEC and droplet formation in trap  $U_C$  are marked “BEC” and “droplet,” respectively.

the quasidegenerate stable ground states, the imaginary-time approach also finds excited states with a specific symmetry, e.g., the parity-antisymmetric square-lattice and honeycomb-lattice states, which could be metastable.

To study the universal nature of the formation of droplets for different  $N$  and different lattice symmetries in trap  $U_C$ , we plot in Figs. 8(a) and 8(b) the energy  $E$  per atom and the number of droplets  $n_d$  versus the corresponding  $N$ . In addition, we plot the energy from Fig. 2(a) of Ref. [39] for one- to seven-droplet states, in arbitrary units, calculated with different trap parameters ( $f_x = f_y = 60$  Hz and  $f_z = 300$  Hz) and a different scattering length,  $a = 70a_0$ . We could reproduce the results of Fig. 2(a) of Ref. [39] using the approximate auxiliary function (8) in place of the exact expression (7) used in this paper. For example, using Eq. (8), for the one-droplet state of Ref. [39] we obtain energy per atom  $E/h \approx 348$  Hz, and for the seven-droplet state we obtain  $E/h \approx 840$  Hz, close to the results illustrated in Fig. 2(a) of Ref. [39]. The use of Eq. (7) leads to much larger energies. From Fig. 8(a) we find the scaling relation between  $E$  and  $N$  in the region of droplet formation ( $N > N_{cr} = 33\,000$  in trap  $U_C$ ),

$$E \approx 0.06 \times N^{0.4}, \quad (13)$$

independent of the lattice symmetry, scattering length  $a$ , and trap parameters. We multiplied the results of Ref. [39] by an arbitrary factor ( $\sim 1.5$ ) to take care of the prefactor in scaling (13); nevertheless, it is remarkable that all points lie on the same universal line and the exponent (0.4) is independent of scattering length and trap parameters. The point with the smallest number of atoms from our calculation in Fig. 8(a) is  $N = 35\,000$  with one droplet. By including the results of Ref. [39], we could include six points with  $N < 40\,000$  containing one to seven droplets covering about one order of magnitude in Fig. 8(a): with the parameters of Ref. [39] one droplet can be generated with a much smaller number  $N = 3980$  of atoms. The points labeled BEC in Fig. 8(a) represent a normal superfluid BEC without droplet formation (see Fig. 2). These points deviate a bit from the universal scaling (13)

valid for droplets, especially for small  $N$ . From Fig. 8(b), with exactly the same points as in Fig. 8(a), the number of droplets  $n_d$  in an arrangement is approximately linearly proportional to  $N$ :  $n_d \approx N/12\,000$ , indicating the average number of 12 000 atoms per droplet; we note that the points generating the large width of the scaling in Fig. 8(b) have collapsed on the straight-line fit (13) in Fig. 8(a). The small difference in energy between the ground and excited states [see Figs. 7 and 5(b)] is not noticeable in Fig. 8(a). We have established the universal nature of scaling (13) in the fact that the exponent is independent of not only the value of  $N$  extended over about two orders of magnitude but also of different parameters of the problem, trap frequencies, and scattering length. It remains to be seen whether this exponent is independent of large variation of the dipole moment or of the details of the beyond-mean-field correction, which stops the collapse. Only after establishing the true universality can the physical origin of the scaling relation be addressed [51], which will be an interesting topic of future investigation.

In this theoretical study we have neglected the effect of the three-body recombination loss of atoms. A matter of concern for the experimental observation [15,42] of a spatially periodic lattice of droplets is the large atom number ( $N \sim 10^5$ ) required, where the effect of the three-body recombination loss of atoms might not be negligible [40]. Nevertheless, a reasonably small value of the loss parameter ( $= 1.25 \times 10^{-41}$  m<sup>6</sup>/s) is estimated for <sup>164</sup>Dy atoms [15,29] from measurements on a thermal cloud and is assumed to be constant over the small range of scattering lengths near  $a = 60\text{--}80a_0$  close to the experimental estimate  $a = 92a_0$  [50] and the value  $a = 85a_0$  used in this study. Considering the upper estimate of  $N = 10^6$  atoms in this study (see Figs. 3 and 4) with a volume of  $40 \times 40 \times 10$  in dimensionless units with length scale  $l = 0.607$   $\mu\text{m}$ , we obtain a typical atomic density of  $3 \times 10^{14}$  cm<sup>-3</sup> =  $3 \times 10^{20}$  m<sup>-3</sup>, which is within the acceptable limit for the formation of droplets in an experiment, as established in previous experimental [15,29] and theoretical [40,42] investigations.

#### IV. SUMMARY

We have demonstrated, using the GP equation including the quantum-fluctuation LHY interaction, supersolid-like spatially periodic crystallization of droplets of a cylindrically symmetric quasi-2D trapped dipolar BEC on square and honeycomb lattices in addition to the triangular-lattice crystallization observed experimentally [14] and studied theoretically [38,39]. There are two possible types of square-lattice crystallization of droplets, e.g., with the central site at  $x = y = 0$  occupied (parity symmetric) or vacant (parity antisymmetric). The parity-symmetric square-lattice crystallization and triangular-lattice crystallization form two quasidegenerate ground states. The parity-antisymmetric square-lattice crystallization and honeycomb-lattice crystallization, both with the central site vacant, form two low-lying excited states. The number of droplets in these lattice arrangements increases with the number of atoms in an approximately linear fashion. We established a robust scaling relation (13) valid for about two orders of magnitude between the energy per atom and the number of atoms in the region of droplet formation, independent of the lattice symmetry (square, honeycomb, or triangular) of droplets, so the three lattice crystalliza-

tions should be of phenomenological interest. The stability of each of these crystallizations can be theoretically established by a linear stability analysis. However, this is a formidable task of future interest, considering the nonlocal nature of dipolar interaction. Nevertheless, both the triangular- and square-lattice structures are close-packed quasidegenerate structures with a predominantly repulsive “interdroplet” interaction and are expected to be stable, whereas the excited honeycomb-lattice structure has an empty site at the center of a hexagon and is conjectured to be unstable. Hence, from an energetic consideration, the parity-symmetric square-lattice crystallization, with the central site at  $x = y = 0$  occupied, is a likely candidate for experimental observation in addition to the already observed triangular-lattice crystallization. The results of this paper can be tested in experiments with strongly dipolar atomic BECs of  $^{164}\text{Dy}$  or  $^{168}\text{Er}$  atoms with present knowhow.

#### ACKNOWLEDGMENTS

S.K.A. acknowledges support from CNPq (Brazil) Grant No. 301324/2019-0 and from ICTP-SAIFR-FAPESP (Brazil) Grant No. 2016/01343-7

- 
- [1] E. P. Gross, *Phys. Rev.* **106**, 161 (1957).  
 [2] A. F. Andreev and I. M. Lifshitz, *Zh. Eksp. Teor. Fiz.* **56**, 2057 (1969) [*Sov. Phys. JETP* **29**, 1107 (1969)].  
 [3] A. J. Leggett, *Phys. Rev. Lett.* **25**, 1543 (1970).  
 [4] G. V. Chester, *Phys. Rev. A* **2**, 256 (1970).  
 [5] M. Boninsegni and N. V. Prokofev, *Rev. Mod. Phys.* **84**, 759 (2012).  
 [6] V. I. Yukalov, *Physics* **2**, 49 (2020).  
 [7] E. Kim and M. H. W. Chan, *Nature (London)* **427**, 225 (2004).  
 [8] S. Balibar, *Nature (London)* **464**, 176 (2010).  
 [9] Z.-K. Lu, Y. Li, D. S. Petrov, and G. V. Shlyapnikov, *Phys. Rev. Lett.* **115**, 075303 (2015).  
 [10] N. Y. Yao, C. R. Laumann, A. V. Gorshkov, S. D. Bennett, E. Demler, P. Zoller, and M. D. Lukin, *Phys. Rev. Lett.* **109**, 266804 (2012).  
 [11] F. Wächtler and L. Santos, *Phys. Rev. A* **93**, 061603(R) (2016).  
 [12] F. Cinti, T. Macrì, W. Lechner, G. Pupillo, and T. Pohl, *Nat. Commun.* **5**, 3235 (2014).  
 [13] Y. Li, G. I. Martone, L. P. Pitaevskii, and S. Stringari, *Phys. Rev. Lett.* **110**, 235302 (2013).  
 [14] H. Kadau, M. Schmitt, M. Wenzel, C. Wink, T. Maier, I. Ferrier-Barbut, and T. Pfau, *Nature (London)* **530**, 194 (2016).  
 [15] M. Schmitt, M. Wenzel, F. Böttcher, I. Ferrier-Barbut, and T. Pfau, *Nature (London)* **539**, 259 (2016).  
 [16] J.-R. Li, J. Lee, W. Huang, S. Burchesky, B. Shteynas, F. Ç. Top, A. O. Jamison, and W. Ketterle, *Nature (London)* **543**, 91 (2017).  
 [17] P. Kaur, S. Gautam, and S. K. Adhikari, *Phys. Rev. A* **105**, 023303 (2022).  
 [18] S. K. Adhikari, *Phys. Rev. A* **103**, L011301 (2021).  
 [19] S. K. Adhikari, *J. Phys.: Condens. Matter* **33**, 265402 (2021).  
 [20] S. K. Adhikari, *J. Phys.: Condens. Matter* **33**, 425402 (2021).  
 [21] L. Chomaz, S. Baier, D. Petter, M. J. Mark, F. Wächtler, L. Santos, and F. Ferlaino, *Phys. Rev. X* **6**, 041039 (2016).  
 [22] F. Wächtler and L. Santos, *Phys. Rev. A* **94**, 043618 (2016).  
 [23] R. N. Bisset, R. M. Wilson, D. Baillie, and P. B. Blakie, *Phys. Rev. A* **94**, 033619 (2016).  
 [24] T. D. Lee, K. Huang, and C. N. Yang, *Phys. Rev.* **106**, 1135 (1957).  
 [25] A. R. P. Lima and A. Pelster, *Phys. Rev. A* **84**, 041604(R) (2011).  
 [26] A. R. P. Lima and A. Pelster, *Phys. Rev. A* **86**, 063609 (2012).  
 [27] G. Semeghini, G. Ferioli, L. Masi, C. Mazzinghi, L. Wolswijk, F. Minardi, M. Modugno, G. Modugno, M. Inguscio, and M. Fattori, *Phys. Rev. Lett.* **120**, 235301 (2018).  
 [28] C. R. Cabrera, L. Tanzi, J. Sanz, B. Naylor, P. Thomas, P. Cheiney, and L. Tarruell, *Science* **359**, 301 (2018).  
 [29] I. Ferrier-Barbut, H. Kadau, M. Schmitt, M. Wenzel, and T. Pfau, *Phys. Rev. Lett.* **116**, 215301 (2016).  
 [30] L. Chomaz, D. Petter, P. Ilzhöfer, G. Natale, A. Trautmann, C. Politi, G. Durastante, R. M. W. van Bijnen, A. Patscheider, M. Sohmen, M. J. Mark, and F. Ferlaino, *Phys. Rev. X* **9**, 021012 (2019).  
 [31] G. Natale, R. M. W. van Bijnen, A. Patscheider, D. Petter, M. J. Mark, L. Chomaz, and F. Ferlaino, *Phys. Rev. Lett.* **123**, 050402 (2019).  
 [32] L. Tanzi, E. Lucioni, F. Famà, J. Catani, A. Fioretti, C. Gabbanini, R. N. Bisset, L. Santos, and G. Modugno, *Phys. Rev. Lett.* **122**, 130405 (2019).  
 [33] F. Böttcher, J.-N. Schmidt, M. Wenzel, J. Hertkorn, M. Guo, T. Langen, and T. Pfau, *Phys. Rev. X* **9**, 011051 (2019).  
 [34] M. Guo, F. Böttcher, J. Hertkorn, J.-N. Schmidt, M. Wenzel, H. P. Büchler, T. Langen, and T. Pfau, *Nature (London)* **574**, 386 (2019).

- [35] L. Tanzi, S. Rocuzzo, E. Lucioni, F. Famà, A. Fioretti, C. Gabbanini, G. Modugno, A. Recati, and S. Stringari, *Nature (London)* **574**, 382 (2019).
- [36] R. Bombin, J. Boronat, and F. Mazzanti, *Phys. Rev. Lett.* **119**, 250402 (2017).
- [37] M. A. Norcia, C. Politi, L. Klaus, E. Poli, M. Sohmen, M. J. Mark, R. Bisset, L. Santos, and F. Ferlaino, *Nature (London)* **596**, 357 (2021).
- [38] E. Poli, T. Bland, C. Politi, L. Klaus, M. A. Norcia, F. Ferlaino, R. N. Bisset, and L. Santos, *Phys. Rev. A* **104**, 063307 (2021).
- [39] D. Baillie and P. B. Blakie, *Phys. Rev. Lett.* **121**, 195301 (2018).
- [40] Y.-C. Zhang, T. Pohl, and F. Maucher, *Phys. Rev. A* **104**, 013310 (2021).
- [41] J. Hertkorn, J.-N. Schmidt, M. Guo, F. Böttcher, K. S. H. Ng, S. D. Graham, P. Uerlings, T. Langen, M. Zwierlein, and T. Pfau, *Phys. Rev. Res.* **3**, 033125 (2021).
- [42] Y.-C. Zhang, F. Maucher, and T. Pohl, *Phys. Rev. Lett.* **123**, 015301 (2019).
- [43] J. Hertkorn, J.-N. Schmidt, M. Guo, F. Böttcher, K. S. H. Ng, S. D. Graham, P. Uerlings, H. P. Büchler, T. Langen, M. Zwierlein, and T. Pfau, *Phys. Rev. Lett.* **127**, 155301 (2021).
- [44] J. Léonard, A. Morales, P. Zupancic, T. Esslinger, and T. Donner, *Nature (London)* **543**, 87 (2017).
- [45] T. Lahaye, C. Menotti, L. Santos, M. Lewenstein, and T. Pfau, *Rep. Prog. Phys.* **72**, 126401 (2009).
- [46] R. Kishor Kumar, L. E. Young-S., D. Vudragović, A. Balaž, P. Muruganandam, and S. K. Adhikari, *Comput. Phys. Commun.* **195**, 117 (2015).
- [47] V. I. Yukalov, *Laser Phys.* **28**, 053001 (2018).
- [48] V. Lončar, L. E. Young-S., S. Škrbić, P. Muruganandam, S. K. Adhikari, and A. Balaž, *Comput. Phys. Commun.* **209**, 190 (2016).
- [49] P. Muruganandam and S. K. Adhikari, *Comput. Phys. Commun.* **180**, 1888 (2009).
- [50] Y. Tang, A. Sykes, N. Q. Burdick, J. L. Bohn, and B. L. Lev, *Phys. Rev. A* **92**, 022703 (2015).
- [51] M. D'Onofrio, P. Marziani, and C. Chiosi, *Front. Astron. Space Sci.* **8**, 694554 (2021).